Supplementary Information for

Vehicle emissions and industrial activities as major sources of methylsiloxanes in urban road dust: A nationwide study in China

Fei Zhang[a], Xinru Luo[a], Haoran Niu[a], Anping Zhang[a], Xianfa Su[a], Jianhui Sun[a], Jing Han[a], Shujie Guo[a], Shuying Dong[a], Zhenwu Tang[b*], Jinglan Feng[a*]

[a]*School of Environment, Henan Normal University, Key Laboratory for Yellow River and Huai River Water Environment and Pollution Control, Ministry of Education, Henan Key Laboratory for Environmental Pollution Control, Xinxiang,Henan 453007, China*

[b]*College of Resources and Environment, Southwest University, Chongqing, 400715, China*

Fei Zhang, E-mail: zhangfei@stu.htu.edu.cn
Xinru Luo, E-mail: luoxinru_htu@163.com
Haoran Niu, E-mail: niuhr_htu@163.com
Anping Zhang,E-mail: zhanganping_htu@163.com
Xianfa Su, E-mail: xfsu8008@126.com
Jianhui Sun,E-mail: sunjhhj@163.com
Han Jing,E-mail: 2822621657@qq.com
Shujie Guo, E-mail: guoshj502@163.com
Shuying Dong, E-mail: dongsy@htu.edu.cn
Zhenwu Tang, E-mail: tangzhenwu@swu.edu.cn
Jinglan Feng, E-mail: fengjinglan@163.com

[*] Corresponding author
E-mail:fengjinglan@163.com, tangzhenwu@swu.edu.cn; Tel: +86 373 3326140; fax: +86 373 3326140.

The Supporting Information contains:

Text S1 Sample preparation and analysis.

1.1. The chromatographic conditions of GC/MS analysis.

The optimum GC/MS conditions were described in our recent report, as well as the conditions for MS operation in selected ion monitoring (SIM) mode (Feng et al., 2018; Niu et al., 2023). The chromatographic conditions for GC/MS were as follows: (1) Splitless injection mode was used (1 μL); the injector temperature was set at 250 °C; the initial temperature of the column was 40 °C (held for 2 min), increased at 20 °C/min to 220 °C, then ramped at 5 °C/min to 290 °C and maintained for 5 min; the auxiliary (also "Aux") temperature was 300 °C. (2) The temperature of the electron ionization (EI) source was 230 °C; the electron energy was 70 eV. GC/MS was run in SIM mode. The chromatograms of the target methylsiloxanes (MSs) are shown in Fig. S1.

1.2. Sample preparation.

The extraction of methylsiloxanes (MSs) from road dust samples was via a modified extraction method (Lu et al., 2010; Sánchez-Brunete et al., 2010; Niu et al., 2023). In short, 1.0 g of sieved dust sample was placed in a 25 mL glass tube and spiked with 100 ng of ^{13}C-labeled D4 and ^{13}C-labeled D5 as surrogate standards. Subsequently, 1.0 g of Na_2SO_4 was added and mixed with the dust sample for 1 min. Ultrasonically-assisted extraction of the spiked dust sample was performed using 5 mL n-hexane in ice-water bath for 5 min. The samples were then centrifuged at 3500 rpm for 5 min at 4°C, after which the solvent layer was transferred into a rotary evaporation flask. Two additional extractions were performed following the aforementioned procedure. The three resulting solvent layers were combined into the same rotary evaporation flask and concentrated to approximately 0.5 mL using a rotary evaporator. The residue was then transferred to a 2 mL vial and spiked with 100

ng M_4Q. The final solution was diluted to 1 mL with n-hexane and immediately passed through a nylon filter (0.22 μm pore size) prior to GC/MS analysis.

1.3. Total organic carbon analysis.

The preparation of the samples for TOC measurement was reported in our previous study (Feng et al., 2019). The TOC content of road dust was determined using a TOC analyser (vario TOC cube, Elementar). The combustion temperature was set at 950°C. A total of 101 road dust samples was analysed.

Text S2 Additional content on Quality assurance and quality control (QA/QC) procedures.

Because MSs are present in environment matrices, consumer products and laboratory products, careful QA/QC precautions included the following: (1) laboratory personnel participating in this study were prohibited from using silicone-containing products such as consumer products; (2) during sampling events, anhydrous sodium sulphate (1 g) as a field blank was exposed in sampling locations to assess the potential ambient contamination; (3) sample pretreatment processes were performed in a clean air cabinet; (4) to avoid contamination from vial caps, no-cap sample vials were purchased and aluminium foil was used as the closure; (5) more than 20 samples of n-hexane were injected consecutively to minimise and stabilise MSs bleeding from capillary columns; and (6) to decrease cross-contamination, additional injections of an empty needle were performed repeatedly throughout each analytical run.

Text S3 Details on Principal component analysis (PCA) and Positive Matrix Factorization (PMF).

PCA. PCA is a multivariate analytical tool used for receptor modelling in environmental source apportionment studies (Sofowote et al., 2008). The major advantage of PCA is that all sources and source profiles need not be known or

predetermined. The concentrations of variables can be regarded as linear combinations of a number of underlying factors (or sources). The task in PCA is to represent the total variability of the original MSs data in a minimum number of factors.

Low detection frequencies (DFs) of analysis factors and unevenly distributed data samples may compromise the effectiveness of PCA. Therefore, L3 and L4, which exhibited extremely low DFs, were excluded from the PCA. Additionally, samples with uneven data distributions—such as those containing only CMSs or only LMSs—were also omitted. Furthermore, PCA relies on inter-variable correlations to achieve effective dimensionality reduction. However, statistical analysis revealed that D3 correlated only with D4; D4 showed no significant correlation with LMSs; L15, L16, and D7 had no mutual correlations; and L16 also showed no significant correlation with D3–D7 (see Table S5). As a result, the methylsiloxanes included in the PCA were limited to D5–D8 and L5–L14, based on a final dataset comprising 139 samples.

In this study, PCA followed by multiple linear regression of the data was performed using SPSS software. Each factor is orthogonal to all others, which results in the smallest possible covariance. The first factor represents the weighted (factor loadings) linear combination of the original variables (i.e., individual MSs) that account for the greatest variability. Each subsequent factor accounts for less variability than the previous. By critically evaluating the factor loadings, an estimate of the chemical source responsible for each factor can be made. The number of significant factors was determined during the stepwise multiple linear regression, which identified those factors that significantly improved the regression between the factors and the measured ΣMSs concentration.

Positive MatrixFactorization (PMF). (1) Data treatment. The input data file consisted of receptor concentration (*Con*) and uncertainty (*Un*) matrices. Measured MS concentrations were entered separately for each deployment at every site. First, those exhibiting uneven data distribution were excluded. Data for non-detected MSs in *Con* were replaced by half the method quantification limit (LOQ). Finally, the input *Con* and *Un* matrices composed of 20 congeners (D3-D8 and L3-L16) × 139 samples.The uncertainties of the input datasets were calculated as follows:

$$Unc = \frac{5}{6} \times LODs \quad \textbf{(1)}$$

$$Unc = \sqrt{(Error\ Fraction \times Conc.)^2 + (0.5 \times LOD)^2} \quad \textbf{(2)}$$

where the *Error Fraction* can be set depending on the uncertainty of measurement. Here, Eq. (1) was adopted if the concentration of individual methylsiloxane was less than the method detection limit (*LOD*). Otherwise, Eq. (2) was adopted (US EPA, 2015).

(2) Base Model Execution. When running the PMF model, follow the recommended steps as described in EPA PMF 4.0 User Guide (5.4 Suggested Order of Operations).The first time PMF is performed on the data set, the input data was analysed via the Concentration/Uncertainty, Concentration Scatter Plot and Data Exceptions screens. Species (D3, D4, L3, L4, L15, L16) with low DFs andlow correlation with all other species were not included in the model operation. The weights of other species are adjusted based on the results of residual analysis (ranging from -3 to 3) and the strength of the correlation between their observed and predicted values. Based on the reported studies on the emission sources of methylsiloxanes in outdoor environments (Horii et al., 2019; Meng et al., 2021), the initial determination of the range for optimizing the number of emission factors is set at 2 to 4. The base

models were run with the number of runs set at 100. Based on the results of residual analysis of the species, the optimal number of factors was determined to be three.

(3) Base Model Error Estimation. The Base Model Displacement method (DISP), Base Model Bootstrap method (BS), and BS-DISP method were executed sequentially to perform error estimation of base run. Error estimation summary is presented Fig. S12. In DISP Summary, the first value in the first line is 0, meaning no error. This indicates that there is no significant rotational ambiguity and that the solution is sufficiently robust to be used. In Bootstrap Summary, mapping over 94% of the factors indicates that the BS uncertainties can be interpreted and the number of factors may be appropriate. Further, BS-DISP Summary in Fig.S13 shows that the solution does not have significant rotational ambiguity and the base model and error estimates can be interpreted.

Text S4 Spatial distribution of MSs in road dust in China.

Fig. S9(a) shows the comparison and distribution of ΣMSs from the eastern coast to the western inland of China. The eight provinces with the highest ΣMS values were Inner Mongolia (median: 1393 ng/g dw; North China), Hunan (1185 ng/g dw; Central China), Shandong (1115 ng/g dw; East China), Guangdong (1018 ng/g dw; South China), Henan (898 ng/g dw; Central China), Shanghai (834 ng/g dw; East China), Xinjiang (784 ng/g dw; Northwest China) and Yunnan (500 ng/g dw; Southwest China). High ΣCMSs values mainly occurred in Inner Mongolia (median: 884 ng/g dw; North China), Xinjiang (699 ng/g dw; Northwest China), Yunnan (467 ng/g dw; Southwest China), Guangdong (418 ng/g dw; South China) and Hunan (392 ng/g dw; Central China). The ΣCMS results were similar to those for ΣMSs. The ΣLMSs concentration was the highest in Hunan (867 ng/g dw; Central China), followed by Shandong (720 ng/g dw; East China), Henan (553 ng/g dw; Central China), Shanghai

(458 ng/g dw; South China) and Inner Mongolia (457 ng/g dw; North China). Interestingly, the trend in ΣLMSs was inconsistent with that of ΣCMSs and ΣMSs with nine sample sites (Henan, Guangxi, Qinghai, Hunan, Shandong, Shanghai, Gansu, Heilongjiang and Zhejiang) having higher concentrations of ΣLMSs than ΣCMSs ($p < 0.05$, Mann–Whitney U test). This result suggested that there was a specific source of LMSs. Overall, although the concentrations of ΣMSs, ΣCMSs and ΣLMSs were not significantly correlated with longitude, scatter plots of ΣMSs, ΣCMSs and ΣLMSs fitted with the locally weighted Scatter plot smoother (LOWESS) lines against longitude initially increased and then showed a decreasing trend from the eastern coast to the western inland of China(see Figs. S9(b)–S9(d)).

Text S5 Traffic conditions.

In this study,most of the sampled roads had four lanes. The traffic volume was calculated as the ratio of the number of vehicles in four lanes to the counting time. In the case of a single lane, a traffic volume greater than 10000 vehicles·day^{-1} was considered to be high-volume traffic conditions(Wei et al., 2020). This traffic volume converted to four lanes was about 40000 vehicles/day (about 100 vehicles/min).

Text S6 Road dust properties.

The TOC values of the road dust samples varied from 0.30 to 12.4% (median 4.28%) (See Fig. S14).

Table S1

Sampling sites and numbers of samples (total, n = 148) in China. Sampling temperature (℃): Temp; Altitude (m): ASL.

City	ID	N	E	ASL	Temp	Date
Kashi	Kashi4	39.467	75.990	1297	9	March 2018
	Kashi5	39.463	75.990	1296	9	
Hami	Hami2	42.822	93.548	774	25	October 2016
	Hami3	42.820	93.546	775	26	
	Hami4	42.824	93.549	777	26	
	Hami5	42.825	93.546	762	28	
Xining	Xining1	36.626	101.770	2224	13	September 2016
	Xining2	36.621	101.775	2260	13	
	Xining3	36.633	101.761	2254	19	
	Xining4	36.628	101.758	2268	21	
	Xining5	36.650	101.757	2243	22	
Kunming	Yunnan1	25.057	102.715	1902	25	September 2016
	Yunnan2	25.061	102.702	1906	25	
	Yunnan3	25.057	102.704	1913	25	
	Yunnan4	25.055	102.700	1909	26	
	Yunnan5	25.050	102.714	1891	22	
Baiyin	Gansu1	36.553	104.179	1724	24	October 2016
	Gansu2	36.549	104.165	1734	25	
	Gansu3	36.546	104.170	1724	24	
	Gansu4	36.546	104.165	1723	25	
	Gansu5	36.539	104.182	1719	26	
Chongqing	Chongqing1	29.614	106.334	292	30	September 2016
	Chongqing2	29.605	106.289	310	33	
	Chongqing3	29.597	106.304	295	33	
	Chongqing4	29.602	106.301	238	32	
	Chongqing5	29.602	106.300	285	32	
Guiyang	Guizhou1	26.461	106.597	1201	25	September 2016
	Guizhou2	26.459	106.583	1225	28	
	Guizhou3	26.459	106.583	1225	20	
	Guizhou4	26.404	106.521	1223	23	
Xianyang	Shaanxi1	34.268	108.060	447	28	September 2016
	Shaanxi2	34.273	108.075	468	28	
	Shaanxi3	34.271	108.076	456	28	

	Shaanxi4	34.263	108.064	454	28	
	Shaanxi5	34.256	108.076	442	28	
	Guangxi1	22.834	108.284	80	17	
	Guangxi2	22.843	108.302	86	24	
Nanning	Guangxi3	22.823	108.334	84	8	December 2017
	Guangxi4	22.816	108.324	79	8	
	Shaanxi1	34.245	108.955	418	9	
	Shaanxi2	34.245	108.957	419	9	
Xi'an	Shaanxi3	34.244	108.955	419	9	January 2018
	Shaanxi4	34.244	108.957	420	9	
	Shaanxi5	34.228	108.957	424	9	
	Hainan1	19.991	110.523	23	28	
Haikou	Hainan2	19.988	110.514	21	28	October 2016
	Hainan3	19.981	110.508	18	28	
	Neimenggu1-1	40.812	111.659	1055	21	
	Neimenggu1-2	40.819	111.668	1085	15	
	Neimenggu1-3	40.824	111.677	1065	11	
Hohhot	Neimenggu2-1	40.812	111.701	1100	12	September 2016
	Neimenggu2-2	40.808	111.694	1054	12	
	Neimenggu2-5	40.814	111.703	1051	13	
	Hunan1	28.171	112.940	36	29	
	Hunan2	28.127	113.010	78	30	
Changsha	Hunan3	28.163	112.945	36	30	August 2016
	Hunan4	28.185	112.960	21	30	
	Hunan5	28.168	112.944	37	30	
	Shanxi1	36.210	113.124	935	18	
	Shanxi2	36.211	113.133	930	18	
Changzhi	Shanxi3	36.212	113.134	931	17	September 2016
	Shanxi4	36.191	113.122	934	19	
	Shanxi5	36.187	113.123	1014	17	
	Guangdong1	23.120	113.410	1	22	
	Guangdong2	23.056	113.357	1	17	
Guangzhou	Guangdong3	23.116	113.401	3	18	December 2017
	Guangdong4	23.120	113.391	6	17	
	Guangdong5	23.061	113.371	2	19	
Xuchang	Xuchang1	34.169	113.462	124	-3	January 2018

	Xuchang2	34.170	113.469	114	-3	
	Xuchang3	34.177	113.473	121	-3	
	Xuchang4	34.158	113.469	119	-3	
	Xuchang5	34.142	113.482	114	-3	
	Xuchang6	34.152	113.463	119	-3	
	Henan1	34.743	113.676	102	35	
	Henan2	34.750	113.676	101	35	
Zhengzhou	Henan3	34.750	113.649	111	33	September 2016
	Henan4	34.763	113.641	104	31	
	Henan5	34.743	113.643	106	28	
Hong Kong	HK1	22.393	114.208	10	18	December 2017
	Hubei1	30.567	114.358	42	30	
	Hubei2	30.555	114.344	21	31	
	Hubei3	30.539	114.342	41	31	
Wuhan	Hubei4	30.519	114.393	25	30	September 2016
	Hubei5	30.481	114.408	37	30	
	Hubei6	30.465	114.431	34	30	
	Hebei1	38.081	114.496	79	34	
	Hebei2	38.088	114.489	79	34	
Shijiazhuang	Hebei3	38.112	114.489	76	33	August 2016
	Hebei4	38.076	114.506	79	32	
	Hebei5	38.076	114.514	79	33	
	Jangxi1	28.714	115.818	32	29	
	Jangxi2	28.714	115.868	28	29	
Nanchang	Jangxi3	28.713	115.771	25	24	September 2016
	Jangxi4	28.726	115.772	26	26	
	Jangxi5	28.725	115.819	27	24	
	Beijing1	39.961	116.359	56	31	
	Beijing2	39.962	116.364	55	20	
	Beijing3	39.957	116.364	56	19	September 2016
	Beijing4	39.952	116.365	53	21	
	Beijing5	39.943	116.350	58	22	
	2017Bei1	39.961	116.359	56	28	
	2017Bei2	39.962	116.364	55	29	
	2017Bei3	39.957	116.364	56	30	September 2017
	2017Bei4	39.952	116.365	53	30	

	2017Bei5	39.943	116.350	58	30	
	Shangdong1	36.682	117.056	50	27	
	Shangdong2	36.683	117.062	39	27	
	Shangdong3	36.696	117.066	41	26	August 2016
	Shangdong4	36.684	117.060	36	26	
	Shangdong5	36.685	117.054	33	26	
Jinan	2017Shan1	28.714	115.818	32	2	December 2017
	2017Shan2	28.714	115.868	28	4	
	2017Shan3	28.713	115.771	25	4	
	2017Shan4	28.726	115.772	26	7	
	2017Shan5	28.725	115.819	27	7	
	Fujian1	24.443	118.106	21	17	January 2018
	Fujian2	24.462	118.110	102	17	
Xiamen	Fujian3	24.446	118.118	81	17	
	Fujian4	24.445	118.121	117	17	
	Fujian5	24.448	118.099	157	17	
	Zhejiang1	29.316	120.123	79	33	
	Zhejiang2	29.329	120.102	66	31	
Hangzhou	Zhejiang3	29.317	120.082	65	32	September 2016
	Zhejiang4	29.333	120.053	75	28	
	Zhejiang5	29.333	120.060	71	31	
	Liaoning1	38.914	121.586	23	-2	January 2018
	Liaoning2	38.880	121.529	17	2	
	Liaoning3	38.922	121.479	71	0	
	Lvshun1	38.780	121.146	8	-1	
Dalian	Lvshun2	38.804	121.161	15	-1	
	Lvshun3	38.787	121.147	10	-1	February 2018
	Lvshun4	38.808	121.259	17	-2	
	Lvshun5	38.789	121.153	30	-2	
	Shanghai1	31.269	121.532	11	12	
	Shanghai2	31.287	121.545	4	12	
Shanghai	Shanghai3	31.290	121.547	4	11	February 2018
	Shanghai4	31.287	121.544	6	12	
	Shanghai5	31.275	121.519	6	12	
	Jilin1	43.849	125.333	216	23	
Changchun	Jilin2	43.884	125.318	225	23	October 2016

Harbin	Jilin3	43.848	125.283	236	23	August 2016
	Jilin4	43.882	125.232	221	23	
	Heilongjiang1	45.759	126.685	131	20	
	Heilongjiang2	45.764	126.694	145	26	
	Heilongjiang3	45.755	126.670	130	26	
	Heilongjiang4	45.776	126.634	126	26	
	Heilongjiang5	45.783	126.629	122	25	
	Heilongjiang6	45.770	126.675	136	23	

Table S2

Information on GDP(10^9 RMB),value added of the secondary industry(VA-SI, 10^9 RMB) and population density of main urban area (PD, people/km^2)in China by region[a]

City	**GDP**	VA-SI	**PD[b]**
Kashi	759.86	191.34	6
Hami	403.68	215.16	8
Xining	1248.17	595.64	8477
Kunming	4300.08	1660.11	1632
Baiyin	442.21	178.11	364
Chongqing	17740.60	7765.38	4458
Guiyang	3157.70	1218.79	6694
Xianyang	2390.97	1385.00	10333
Nanning	3703.39	1426.50	151
Xi'an	1248.17	2200.36	6678
Haikou	1257.67	233.56	26176
Hohhot	3173.73	5579.77	1542
Changsha	9455.36	4513.28	7428
Changzhi	1270.48	646.94	13309
Guangzhou	19547.44	5813.45	6176
Xuchang	2377.71	1398.53	268
Zhengzhou	8025.31	3796.93	4507
Hong Kong	24904.38	1449.97	36890
Wuhan	11912.61	5227.05	5841
Shijiazhuang	5927.73	2693.92	1872
Nanchang	4354.99	2307.70	7990
Beijing	25669.10	4665.80	9826
Jinan	6536.12	2368.90	16786
Xiamen	3784.27	1558.62	1270
Hangzhou	11313.72	4120.93	675
Dalian	6730.33	2849.85	83738
Shanghai	28178.70	7794.34	21910
Changchun	5917.94	2926.20	1446
Harbin	6101.61	1896.66	1314

a: Data of GDP, VA-SI and population was obtained from EPS Data (http://olap.epsnet.com.cn/).

b: Population density for each sampling site was obtained by dividing the population of the belonging city or country by the area.

Table S3

The mass spectrometric parameters, standard curves, correlation coefficients, LODs, LOQs, and recoveries of target methylsiloxanes.

Names	Abbreviation	Retention time (min)	Quantitative ion (m/z)	Qualitative ion (m/z)	Standard curve	Correlation coefficient (R^2)	IDL (ng/mL)	IQL (ng/mL)	LOD (ng/g)	LOQ (ng/g)	Recovery (%)
Hexamethylcyclotrisiloxane	D3	4.65	207	207,191,133,96	Y=0.016641X+0.306843	0.9991	2.04	3.06	0.24	0.35	57.7±0.6
Octamethylcyclotetrasiloxane	D4	6.36	281	281,265,207,133	Y=0.018690X+0.418161	0.9992	2.06	3.09	0.16	0.24	86.9±7.9
Decamethylcyclopentasiloxane	D5	7.67	355	355,267, 154, 73	Y=0.007716X+0.163131	0.9995	2.10	3.15	0.18	0.27	76.5±7.1
Dodecamethylcyclohexasiloxane	D6	8.96	341	429, 341, 147,73	Y=0.006549X+0.162914	0.9993	2.02	3.05	0.14	0.22	93.4±12.7
Tetradecamethylcycloheptasiloxane	D7	10.1	281	503,281, 147, 73	Y=9.214045E-004X+0.098961	0.9991	2.24	3.36	0.18	0.27	81.6±6.2
Hexadecamethylcyclooctasiloxane	D8	11.1	355	355, 281,221,73	Y=0.004055X+0.053275	0.9997	1.67	3.34	0.12	0.23	96±6.86
Octamethyltrisiloxane	L3	5.27	221	221, 205, 103,73	Y=0.011430X-0.009001	0.9995	1.03	1.25	0.08	0.10	85.7±12.2
Odecamethylpentasiloxane	L4	6.97	207	295, 207, 191,73	Y=0.016454X-0.011527	0.9994	0.71	1.07	0.05	0.08	90.7±5.3
Dodecamethylpentasiloxane	L5	8.35	281	369, 281, 147,73	Y=0.008196X-0.041771	0.9992	0.68	1.02	0.05	0.07	93.5±5.7
Tetradecamethylcycloheptasiloxane	L6	9.52	355	355,281,221,147	Y=0.005984X-0.117632	0.9993	1.23	1.84	0.09	0.13	93.1±8.2
Hexadecamethylheptasiloxane	L7	10.5	221	295, 221, 147,73	Y=0.006407X-0.147430	0.9996	1.52	2.28	0.11	0.16	93.4±8.9
Octadecamethylnonasiloxane	L8	11.5	221	295,221,207,147	Y=0.004946X-0.163978	0.9992	1.30	1.95	0.09	0.14	95.1±8.8
Eicosamethylnonasiloxane	L9	12.5	221	295,221,207,147	Y=0.004767X-0.143571	0.9993	1.09	1.64	0.08	0.12	93.1±8.1
Docosamethyldecasiloxane	L10	13.7	221	295,281,221,147	Y=0.004037X-0.121005	0.9994	0.90	1.35	0.06	0.10	92.6±7.0
Tetracosamethylundecasiloxane	L11	15.0	221	295,281,221,147	Y=0.002982X-0.045723	0.9996	1.43	2.15	0.10	0.15	92.9±6.1
Hexacosamethyldodecasiloxane	L12	16.7	221	295,281,221,147	Y=0.002161X-0.022350	0.9991	1.43	2.15	0.11	0.16	90.4±5.1
Octacosamethyltridecasiloxane	L13	18.4	221	295,281,221,147	Y=0.001577X-0.015865	0.9995	0.89	1.29	0.07	0.10	89.3±2.3
Triacontamethyltetradecasiloxane	L14	20.3	221	295,221, 147,73	Y=0.001163X-0.006931	0.9996	0.68	1.02	0.05	0.08	88.0±0.1
Dotriacontmethylpentadecasiloxane	L15	22.1	221	295,221, 147,73	Y=8.527201E-004X-0.002893	0.9995	0.86	1.29	0.07	0.10	86.4±4.1
Tetraiacontamethylhexadecasiloxane	L16	23.9	221	295,221,207,147	Y=6.155460E-004X-0.001707	0.9992	1.15	1.73	0.10	0.15	78.1±5.7
	M4Q	7.92	281	369,281,147, 73							
	^{13}C-D4	6.36	288	288, 212	Y=0.018690X+0.218161	0.9991	0.54	1.04	0.04	0.08	88.9±6.8
	^{13}C-D5	7.67	364	364, 272, 76	Y=0.007716X+0.103131	0.9992	0.63	1.22	0.05	0.09	86.5±6.1

Note: IDL, instrument detection limit; IQL, instrument quantification limit; LOD, method detection limit; LOQ, method quantification limit.

Table S4

Concentrations (ng/g dw; rang, median, and mean) and detection frequencies (DFs, %) of methylsiloxanes in road dust (n = 148).

Compound	Range	Median	DF
D3	<LOQ to 89.1	<LOQ	37.8
D4	<LOQ to 81.5	<LOQ	47.3
D5	<LOQ to 180	16.9	81.1
D6	<LOQ to 226	27.0	85.1
D7	<LOQ to 1277	77.4	81.8
D8	<LOQ to 830	18.2	89.9
L3	<LOQ to 1.65	<LOQ	0.70
L4	<LOQ to 1.09	<LOQ	1.40
L5	6.17 to 12.1	6.71	100
L6	<LOQ to 19.1	<LOQ	52.0
L7	<LOQ to 48.5	3.14	73.6
L8	<LOQ to 328	7.65	92.6
L9	<LOQ to 185	12.0	91.2
L10	<LOQ to 3476	11.7	93.9
L11	<LOQ to 399	6.58	81.8
L12	<LOQ to 532	19.1	90.5
L13	<LOQ to 521	7.28	75.7
L14	<LOQ to 431	6.54	53.4
L15	<LOQ to 526	<LOQ	30.4
L16	<LOQ to 7517	<LOQ	23.6
ΣCMSs	<LOQ to 1725	171	
ΣLMSs	6.21 to 8500	87.7	
ΣMSs	6.36 to 8618	336	

<LOQ, below the method quantification limit; ΣCMSs, the sum of D3–D8; ΣLMSs, the sum of L3–L16; ΣMSs, the sum of D3–D8 and L3–L16.

Table S5

Spearman's correlations among methylsiloxanes in road dust samples from China.

Correlations

			D3	D4	D5	D6	D7	D8	L5	L6	L7	L8	L9	L10	L11	L12	L13	L14	L15
Spearman's rho	D4	Correlation Coefficient	.261**																
		Sig. (2-tailed)	.001																
		N	148																
	D5	Correlation Coefficient	.134	.401**															
		Sig. (2-tailed)	.103	.000															
		N	148	148															
	D6	Correlation Coefficient	.160	.212**	.382**														
		Sig. (2-tailed)	.052	.010	.000														
		N	148	148	148														
	D7	Correlation Coefficient	.270**	.183*	.192*	.666**													
		Sig. (2-tailed)	.001	.026	.019	.000													
		N	148	148	148	148													
	D8	Correlation Coefficient	.291**	.168*	.160	.406**	.780**												
		Sig. (2-tailed)	.000	.041	.052	.000	.000												
		N	148	148	148	148	148												
	L5	Correlation Coefficient	.079	.031	.476**	.277**	.293**	.284**											
		Sig. (2-tailed)	.339	.708	.000	.001	.000	.000											
		N	148	148	148	148	148	148											
	L6	Correlation Coefficient	.039	-.020	.220**	.216**	.254**	.329**	.547**										
		Sig. (2-tailed)	.641	.811	.007	.008	.002	.000	.000										
		N	148	148	148	148	148	148	148										
	L7	Correlation Coefficient	.055	-.005	.173*	.171*	.277**	.442**	.555**	.690**									
		Sig. (2-tailed)	.504	.954	.036	.038	.001	.000	.000	.000									
		N	148	148	148	148	148	148	148	148									
	L8	Correlation Coefficient	.051	.036	.210*	.160	.232**	.421**	.492**	.608**	.941**								
		Sig. (2-tailed)	.536	.664	.010	.052	.005	.000	.000	.000	.000								
		N	148	148	148	148	148	148	148	148	148								
	L9	Correlation Coefficient	.098	.010	.139	.242**	.285**	.469**	.389**	.537**	.832**	.852**							

	Sig. (2-tailed)	.234	.908	.091	.003	.000	.000	.000	.000	.000	.000							
	N	148	148	148	148	148	148	148	148	148	148							
L10	Correlation Coefficient	.042	-.001	.151	.160	.195*	.377**	.390**	.551**	.867**	.891**	.890**						
	Sig. (2-tailed)	.609	.991	.067	.052	.018	.000	.000	.000	.000	.000	.000						
	N	148	148	148	148	148	148	148	148	148	148	148						
L11	Correlation Coefficient	.050	-.001	.167*	.099	.164*	.377**	.410**	.565**	.832**	.860**	.836**	.868**					
	Sig. (2-tailed)	.550	.989	.043	.233	.046	.000	.000	.000	.000	.000	.000	.000					
	N	148	148	148	148	148	148	148	148	148	148	148	148					
L12	Correlation Coefficient	-.001	.015	.150	.151	.134	.319**	.358**	.486**	.768**	.803**	.806**	.901**	.780**				
	Sig. (2-tailed)	.990	.852	.068	.066	.105	.000	.000	.000	.000	.000	.000	.000	.000				
	N	148	148	148	148	148	148	148	148	148	148	148	148	148				
L13	Correlation Coefficient	.056	.036	.176*	.108	.164*	.350**	.350**	.494**	.797**	.848**	.818**	.892**	.884**	.855**			
	Sig. (2-tailed)	.501	.660	.033	.190	.047	.000	.000	.000	.000	.000	.000	.000	.000	.000			
	N	148	148	148	148	148	148	148	148	148	148	148	148	148	148			
L14	Correlation Coefficient	.098	-.058	.215**	.221**	.230**	.299**	.431**	.380**	.450**	.433**	.500**	.470**	.548**	.394**	.456**		
	Sig. (2-tailed)	.234	.486	.009	.007	.005	.000	.000	.000	.000	.000	.000	.000	.000	.000	.000		
	N	148	148	148	148	148	148	148	148	148	148	148	148	148	148	148		
L15	Correlation Coefficient	.128	-.035	.262**	.190*	.107	.221**	.445**	.534**	.563**	.564**	.530**	.578**	.568**	.595**	.564**	.585**	
	Sig. (2-tailed)	.122	.669	.001	.021	.194	.007	.000	.000	.000	.000	.000	.000	.000	.000	.000	.000	
	N	148	148	148	148	148	148	148	148	148	148	148	148	148	148	148	148	
L16	Correlation Coefficient	.045	-.008	.102	.085	.109	.277**	.295**	.498**	.555**	.581**	.567**	.639**	.621**	.627**	.660**	.520**	.696**
	Sig. (2-tailed)	.585	.921	.215	.305	.189	.001	.000	.000	.000	.000	.000	.000	.000	.000	.000	.000	.000
	N	148	148	148	148	148	148	148	148	148	148	148	148	148	148	148	148	148

**. Correlation is significant at the 0.01 level (2-tailed).

*. Correlation is significant at the 0.05 level (2-tailed).

N. Number of samples.

Table S6

Varimax-rotated component matrix[a] following principal component analysis of road dust across China (values > 0.5 are highlighted)

	Component		
	1	2	3
L13	**0.961**	0.034	0.064
L11	**0.954**	0.135	0.049
L12	**0.936**	0.106	0.04
L9	**0.913**	0.188	0.131
L14	**0.911**	0.088	0.102
L10	**0.787**	0.152	-0.021
L7	**0.713**	0.436	0.058
L8	**0.507**	0.287	0.084
L5	0.014	**0.881**	-0.068
L6	0.383	**0.745**	-0.028
D5	0.126	**0.533**	0.119
D7	-0.04	-0.02	**0.909**
D8	0.093	-0.09	**0.786**
D6	0.137	0.213	**0.702**

Extraction Method: Principal Component Analysis.

Rotation Method: Varimax with Kaiser Normalization.

a. Rotation converged in 4 iterations.

Table S7

Model summary[d] of multiple linear regression analysis of factor scores variables versus ΣMSs values

Model	R	R Square	Adjusted R Square	Std. Error of the Estimate	Durbin-Watson

1	.708[a]	0.501	0.497	397.8121		
2	.946[b]	0.894	0.893	183.6899		
3	.960[c]	0.922	0.92	158.4033	2.21	

a. Predictors: (Constant), REGR factor score1 for analysis 2;

b. Predictors: (Constant), REGR factor score1 for analysis 2, REGR factor score3 for analysis 2;

c. Predictors: (Constant), REGR factor score1 for analysis 2, REGR factor score3 for analysis 2, REGR factor score2 for analysis 2;

d. Dependent Variable: ΣMSs.

Table S8

ANOVA [a] of multiple linear regression analysis of factor scores variables versus ΣMSs values

Model		**Sum of Squares**	**df**	**Mean Square**	**F**	**Sig.**
1	Regression	21756522	1	21756522	137.478	.000[b]
	Residual	21680862	137	158254.5		
	Total	43437384	138			

2	Regression	38848475	2	19424237	575.67	.000[c]
	Residual	4588910	136	33741.98		
	Total	43437384	138			
3	Regression	40050016	3	13350005	532.05	.000[d]
	Residual	3387368	135	25091.62		
	Total	43437384	138			

a. Dependent Variable: ΣMSs;

b. Predictors: (Constant), REGR factor score1 for analysis 2;

c. Predictors: (Constant), REGR factor score1 for analysis 2, REGR factor score3 for analysis 2;

d. Predictors: (Constant), REGR factor score1 for analysis 2, REGR factor score3 for analysis 2, REGR factor score2 foranalysis 2.

Table S9

Coefficients[a] of multiple linear regression analysis of factor scores variables versus ΣMSs values

Model	Unstandardized Coefficients		Standardized Coefficients	t	Sig.
	B	Std. Error	Beta		
1(Constant)	561.605	33.742		16.644	0
REGR factor score1 for analysis 2	397.059	33.864	0.708	11.725	0
2(Constant)	561.605	15.58		36.046	0
REGR factor score 1 for analysis 2	397.059	15.637	0.708	25.393	0
REGR factor score3 for analysis 2	351.93	15.637	0.627	22.507	0
3(Constant)	561.605	13.436		41.8	0
REGR factor score 1 for analysis 2	397.059	13.484	**0.708**	29.446	0
REGR factor score 3 for analysis 2	351.93	13.484	**0.627**	26.099	0
REGR factor score 2 for analysis 2	93.31	13.484	**0.166**	6.92	0

a. Dependent Variable: ΣMSs.

Table S10

Factor Profiles (% of species sum) from Base Run #1 (Convergent Run) by PMF

Source	Factor 1	Factor 2	Factor 3
D5	1.78	0.0663	**98.2**
D6	**67.2**	9.53	23.3
D7	**92.2**	1.65	6.13
D8	**81.0**	11.7	7.29
L5	20.8	19.6	**59.7**
L6	12.9	**48.4**	38.7
L7	9.34	**67.2**	23.4
L8	5.13	**77.8**	17.0
L9	5.00	**84.9**	10.1
L10	2.82	**87.9**	9.28
L11	1.97	**90.4**	7.64
L12	2.51	**89.1**	8.35
L13	1.65	**91.0**	7.39
L14	37.2	38.9	23.9
Estimated sources	Vehicle emissions	Industrial activities	Use of PCCPs

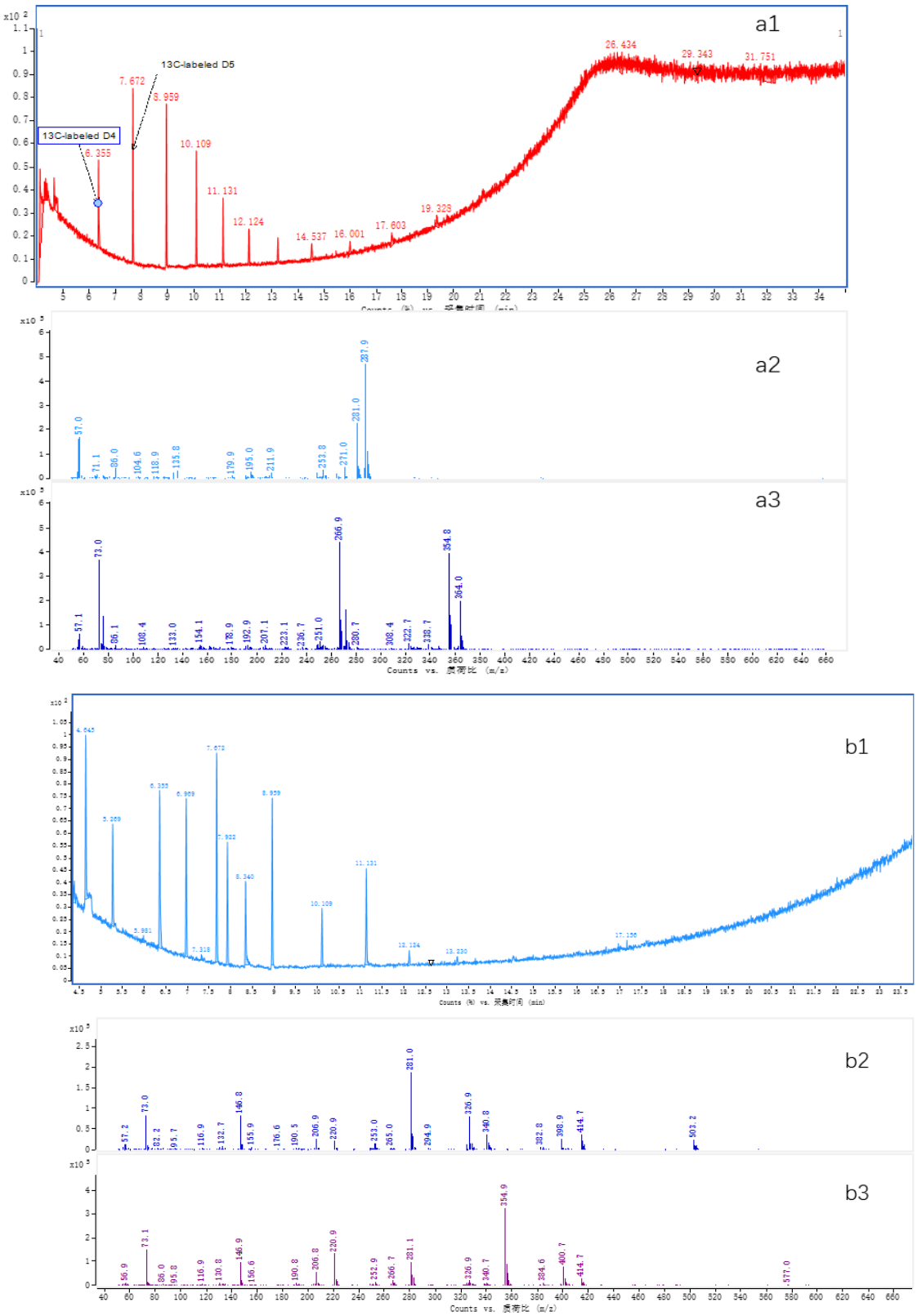
a1
13C-labeled D5
13C-labeled D4
7.672
8.959
6.355
10.109
11.131
12.124
14.537
16.001
17.603
19.328
26.434
29.343
31.751
a2
a3
b1
b2
b3
Counts vs. 质荷比 (m/z)

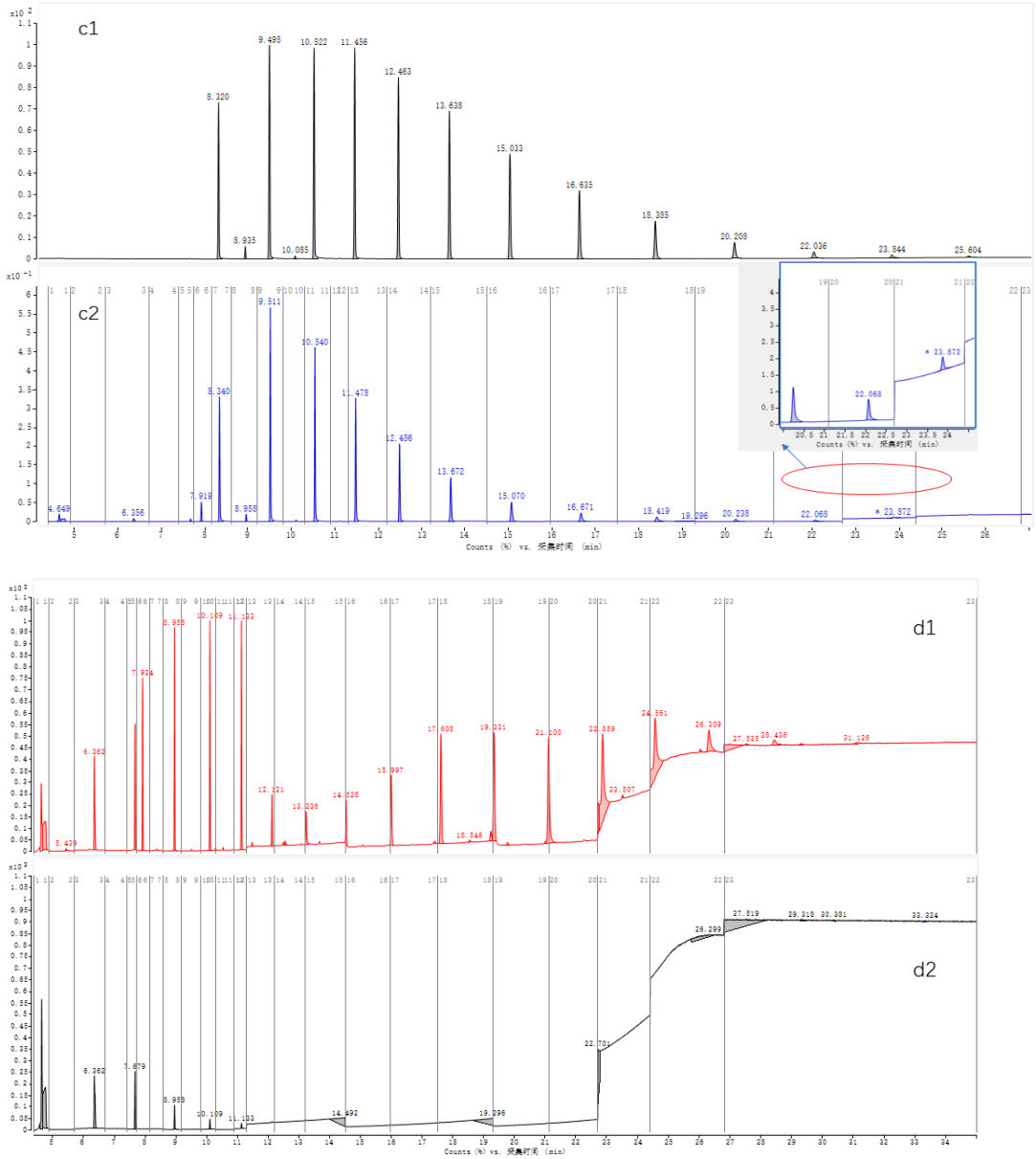

Fig. S1 TIC chromatograms and mass spectrums of methylsiloxanes. 1) TIC chromatograms (a1) and mass spectrums of ^{13}C-labeled-D4 (a2) and ^{13}C-labeled-D5 (a3) in scan mode (100 ng·mL^{-1}); 2) TIC chromatogram of D3–D8, L3–L6 and M4Q was showed in b1; mass spectrums of D7 and D8 were showed in b2 and b3 respectively (100 ng·mL^{-1}); 3) TIC chromatograms of polydimethylsiloxane mixture (PDMS, viscosity of 5 cSt) including L5-L16 wereshowed in c1 (scan mode, 300 μg·mL^{-1}) and c2 (SIM mode, 10 μg·mL^{-1}); 4) The complete chromatograms of target methylsiloxanes for real sample (Xinjiang) (d1) and for n-hexane (d2).

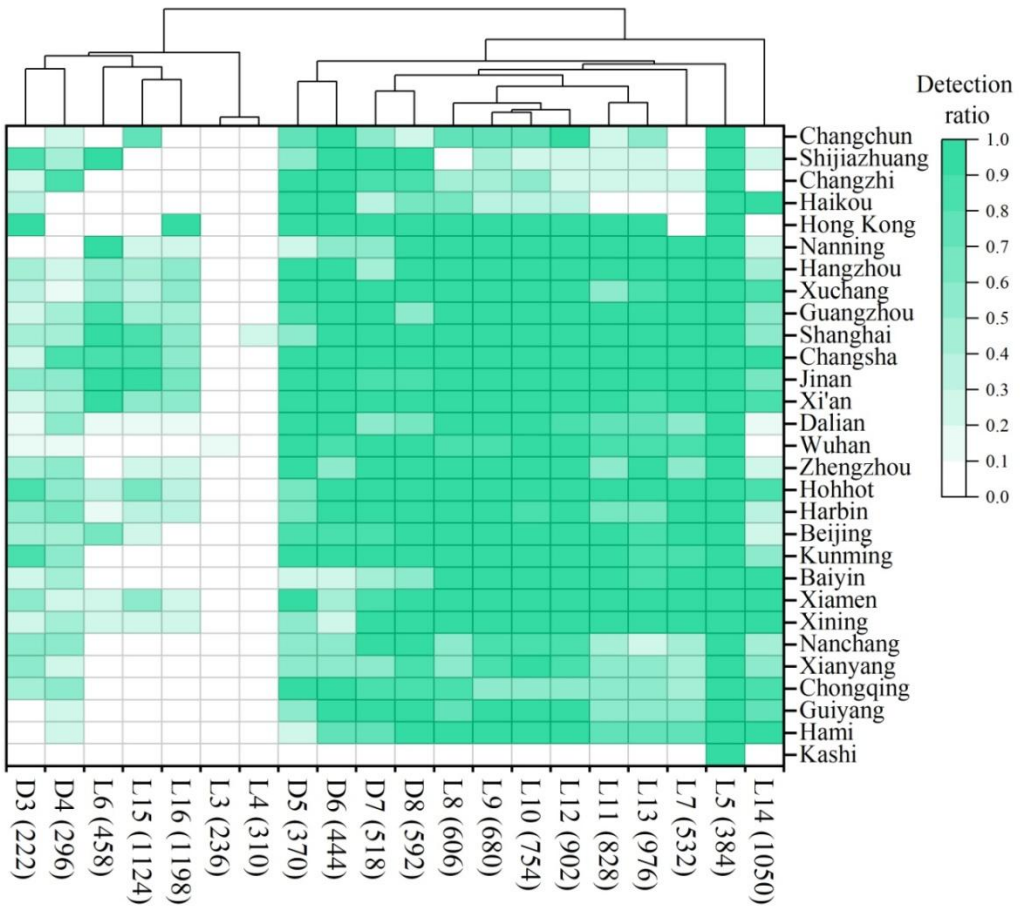

Fig. S2 Heatmap of correlation coefficients and hierarchical clustering analysis of detection ratio of methylsiloxanes in road dust samples.

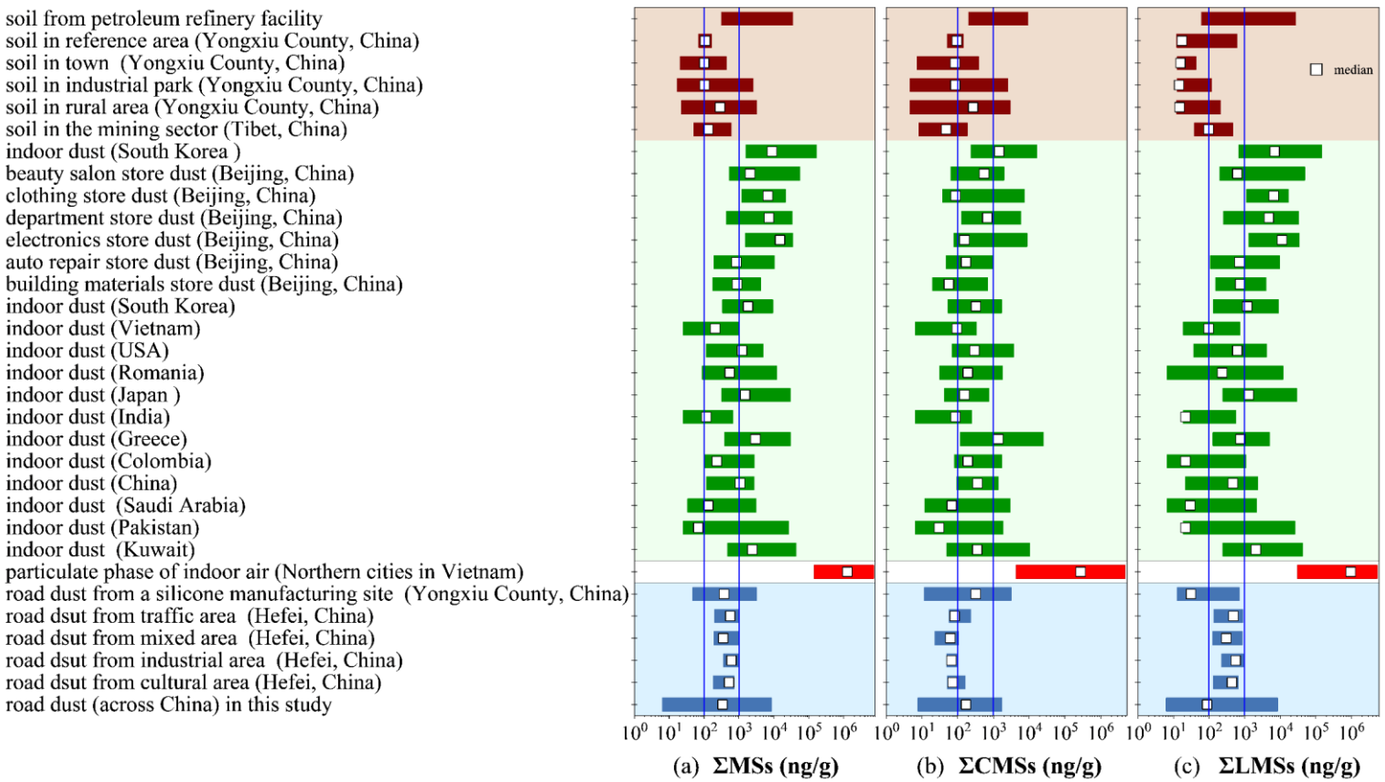

Fig. S3 Concentration ranges (ng/g) of total methylsiloxanes (D3–D7 and L3–L16, ΣMSs) in road dust, particulate phase of indoor air, indoor dust and soil. The road dust was collected from Hefei in China and Yongxiu County in China(Cheng et al., 2021a; Meng et al., 2021), the particulate phase of indoor air was collected from Vietnam(Tran et al., 2018), the indoor dust was collected from twelve countries (indoor dust samples including cars collected from Kuwait, Pakistan and Saudi Arabia)(Tran et al., 2015), the indoor store dust was collected from Beijing, China(Zhu et al., 2023), the indoor dust in homes was collected from South Korea(Chen et al., 2023), the surface soil was collected from Jiama mining sector in Tibet, China(Li et al., 2024), and the soil was collected from a large silicone manufacturing site Yongxiu County, China(Cheng et al., 2021b), and a petroleum refinery facility in Dongying City, China(Liu et al., 2021).

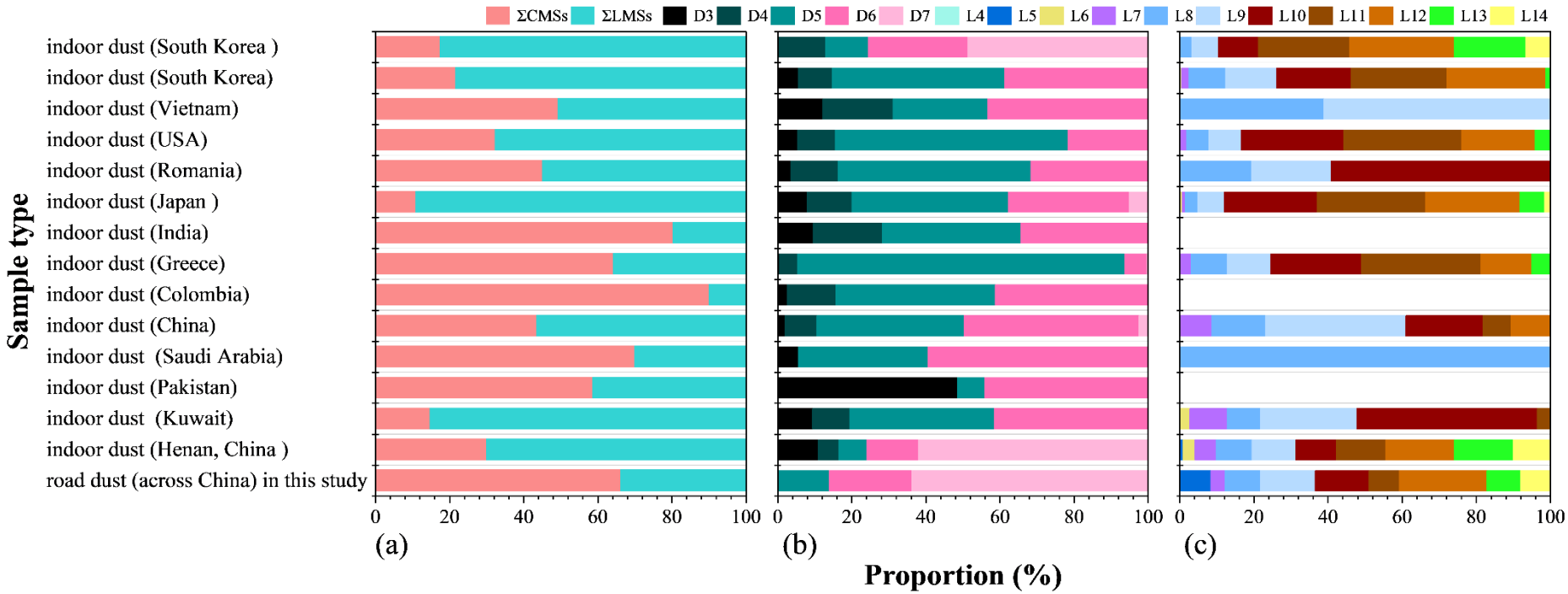

Fig. S4 Comparison of compositional profiles of methylsiloxanes between road dust and the indoor dust reported by Tral et al. (Tran et al., 2015) and Chen et al. (Chen et al., 2023). (A) Proportions of ΣCMSs and ΣLMSs to ΣMSs. (B) Proportions of individual CMSs to ΣCMSs. (C) Proportions of individual LMSs to ΣLMSs.

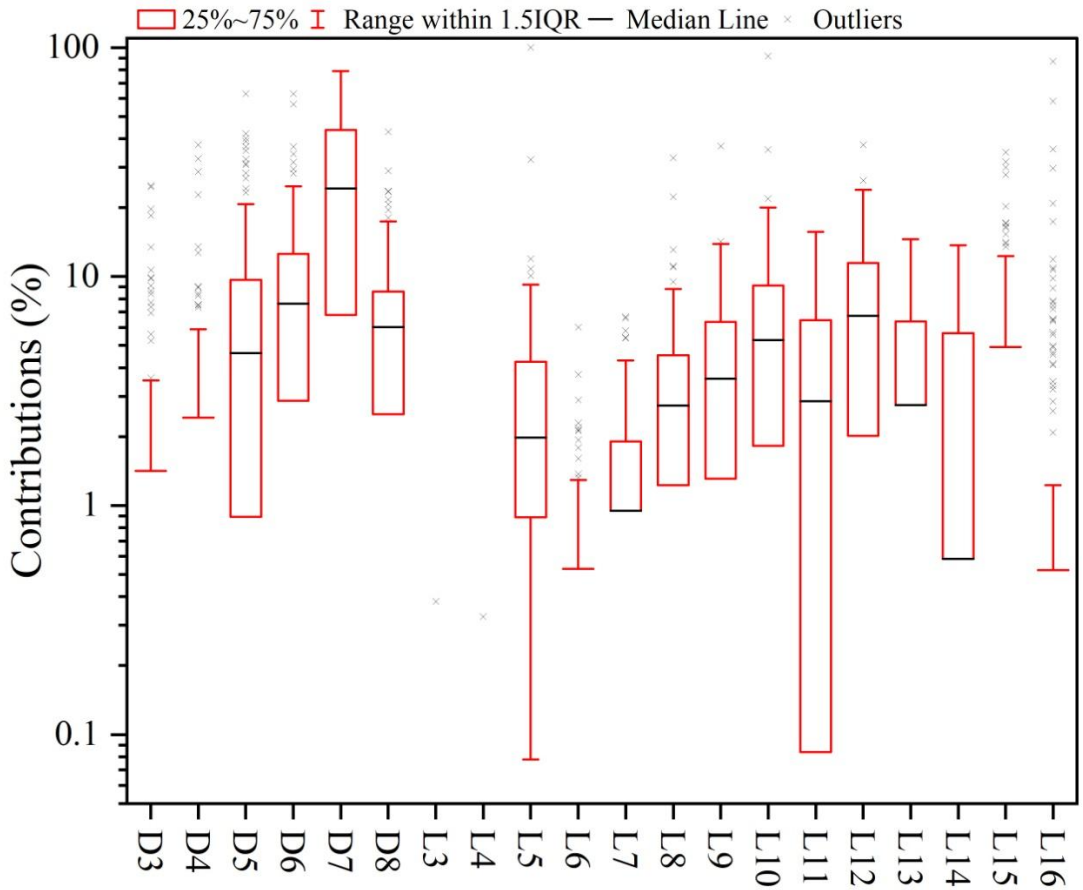

Fig. S5 Contributions of individual MSs to ΣMSs in road dust.

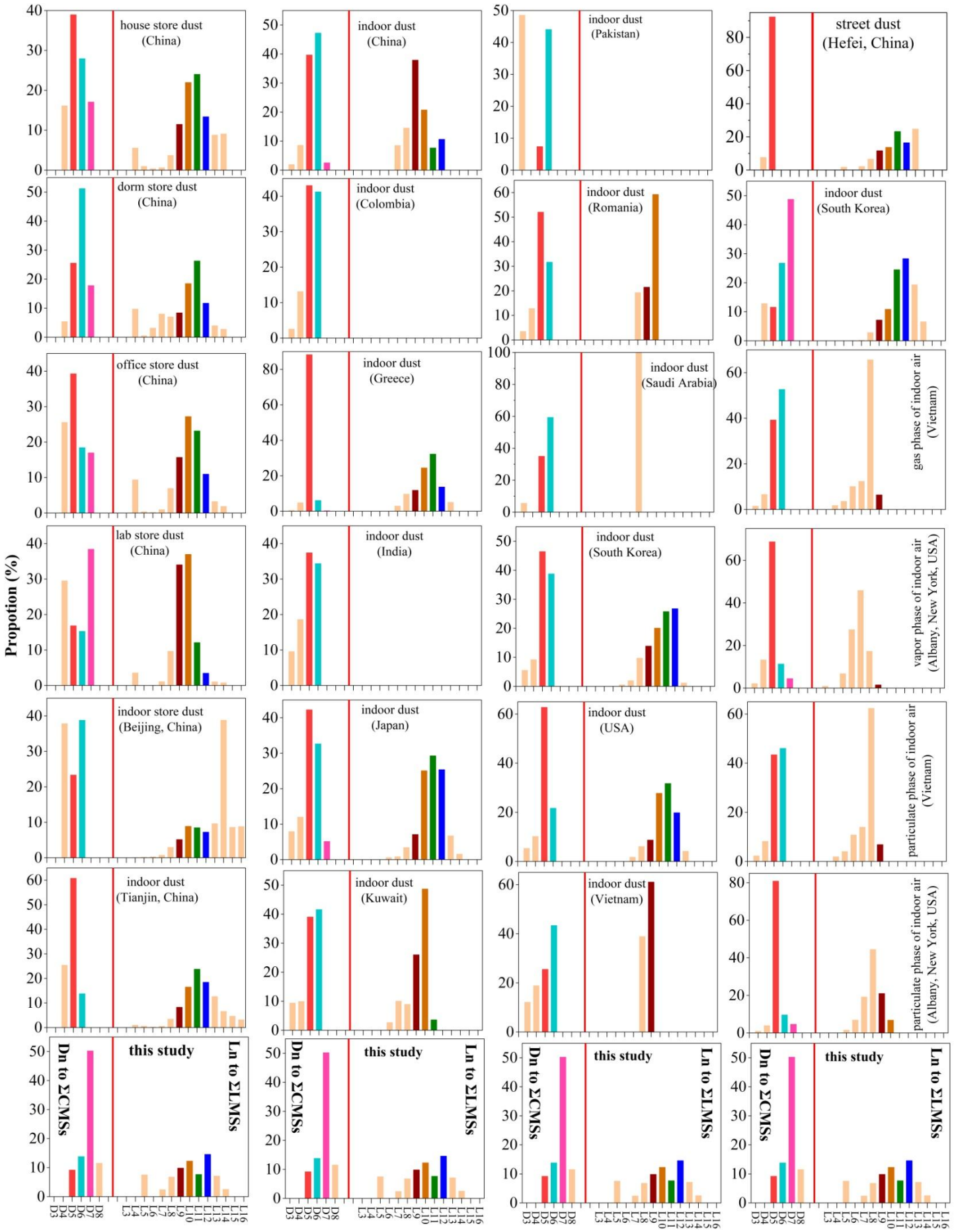

Fig. S6 Comparison of individual cyclic methylsiloxanes to ΣCMSs and individual linear methylsiloxanes to ΣLMSs among road dust in this study, indoor dust (Tran et al., 2015; Chen et al., 2023; Zhu et al., 2023), road dust from Hefei, China (Meng et al., 2021), the particulate phase of indoor air (Tran et al., 2018), and the particulate and vapor phases of indoor air (Tran and Kannan, 2015).

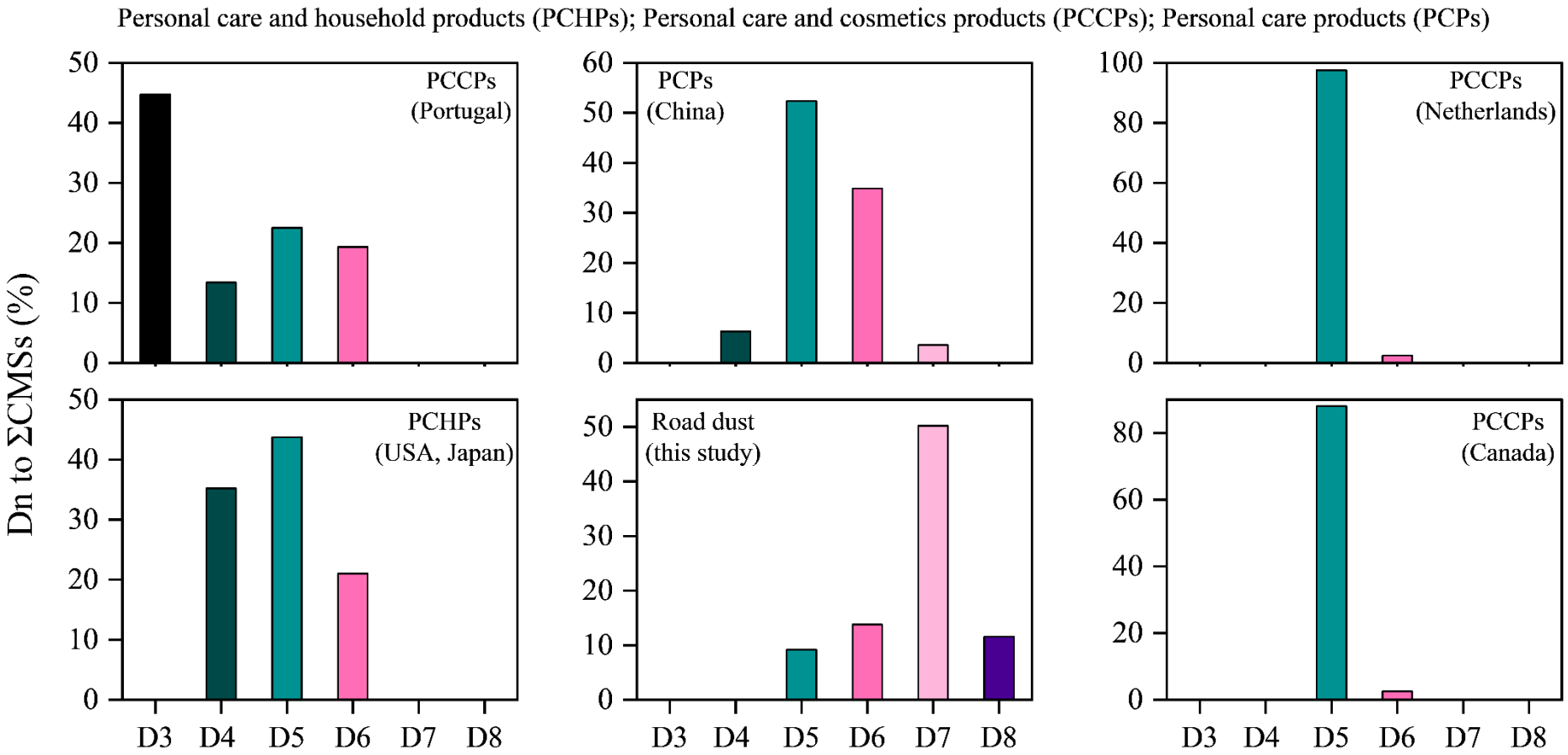

Fig. S7 Comparison of individual cyclic methylsiloxanes to ΣCMSs between road dust in this study and personal care products. Data: PCCPs from Portugal reported by Capela et al.(Capela et al., 2016); PCPs from China reported by Lu et al.(Lu et al., 2011); PCCPs from Netherlands reported by Dudzinaet al.(Dudzina et al., 2014); PCHPs from USA and Japan reported by Horii et al.(Horii and Kannan, 2008); PCCPs from Canada reported by Wanget al.(Wang et al., 2009).

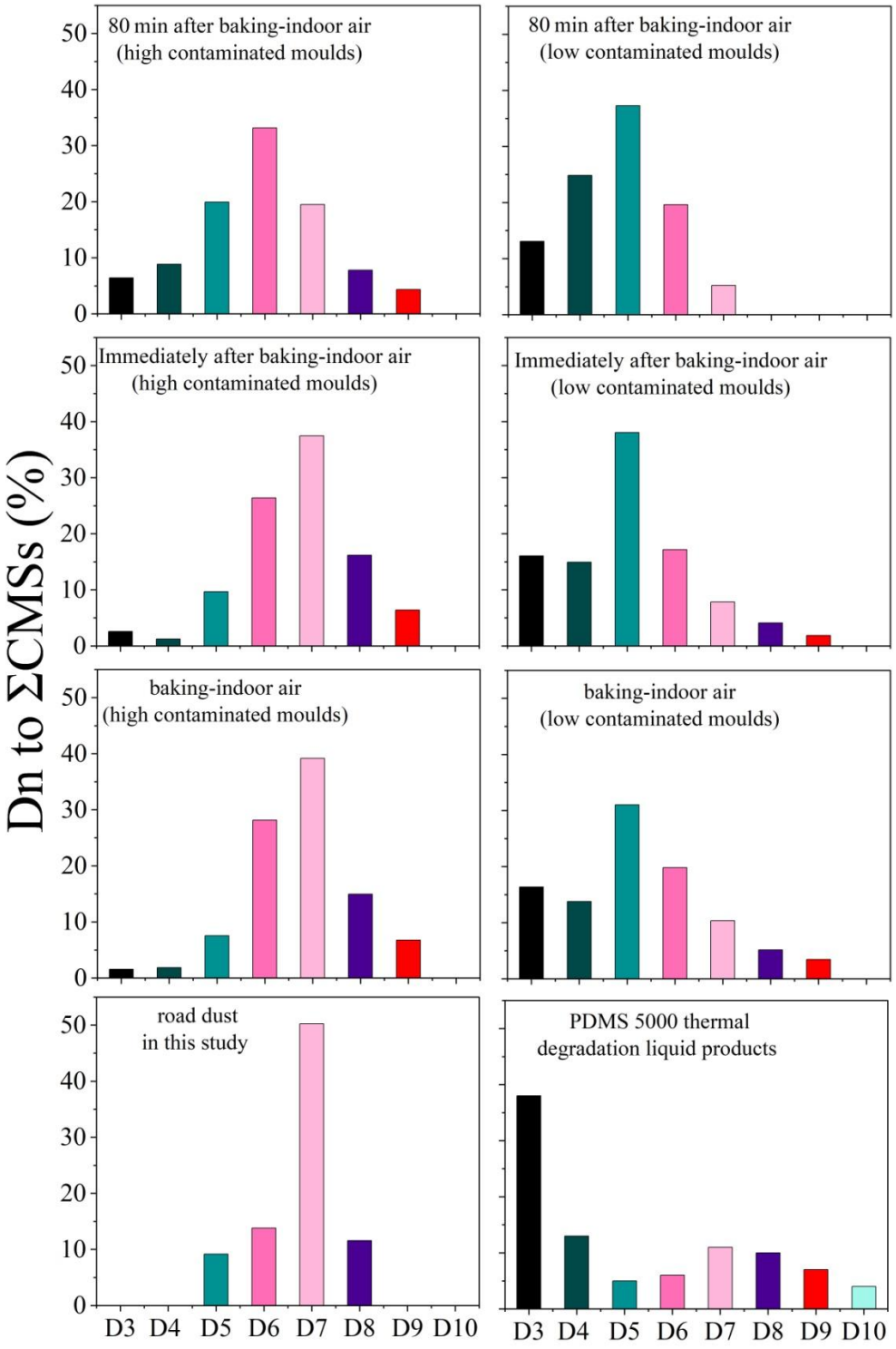

Fig. S8 Comparison individual cyclic methylsiloxanes to ΣCMSs inthermal degradation products of silicone baking moulds (Fromme et al., 2019) and polydimethylsiloxane (PDMS)(Wang et al., 2024) with those in road dust.

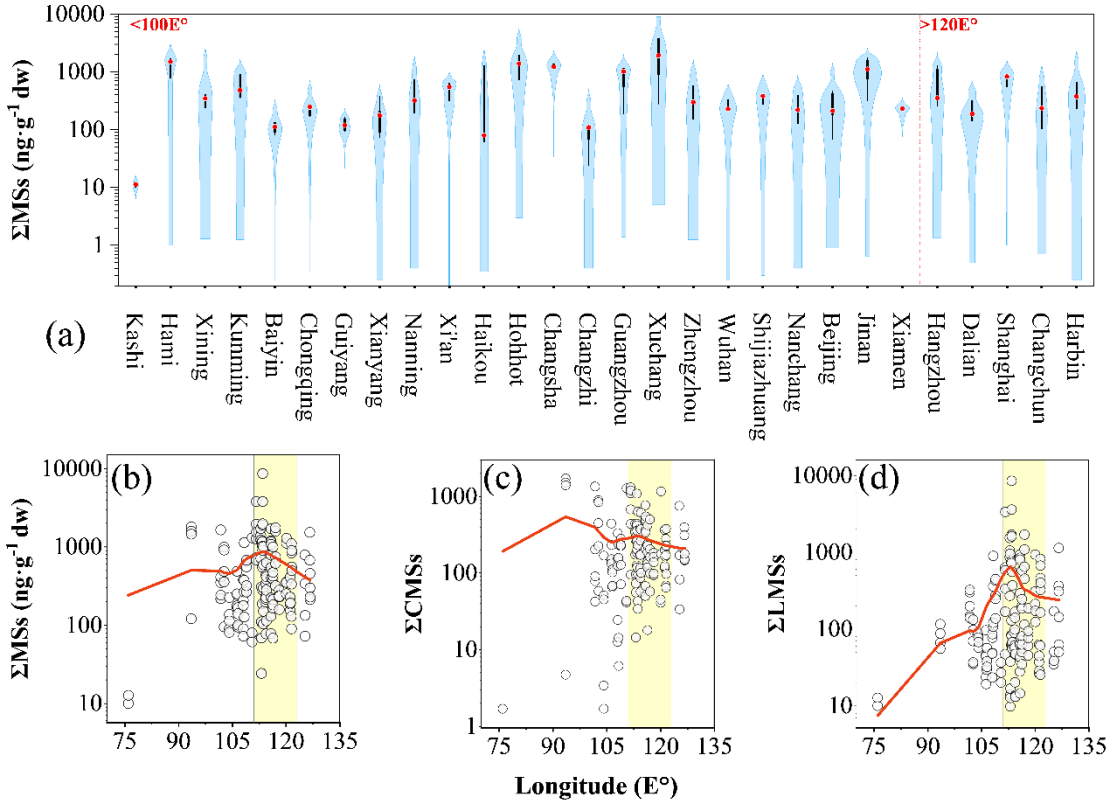

Fig. S9 Large-scale distribution, trend and comparison of the total concentrations of methylsiloxanes, including cyclic and linear methylsiloxanes (ΣMSs: ΣCMSs and ΣLMSs, ng/g dw) in road dust in China. (a) ΣMSs in the road dust of sampled cities distributed from the western inland to the eastern coast of China.(b)-(d) Scatter plot with the fitted LOESS line of the concentrations (ng/g dw) of ΣMSs, ΣCMSs and ΣLMSs in the road dust along longitude.

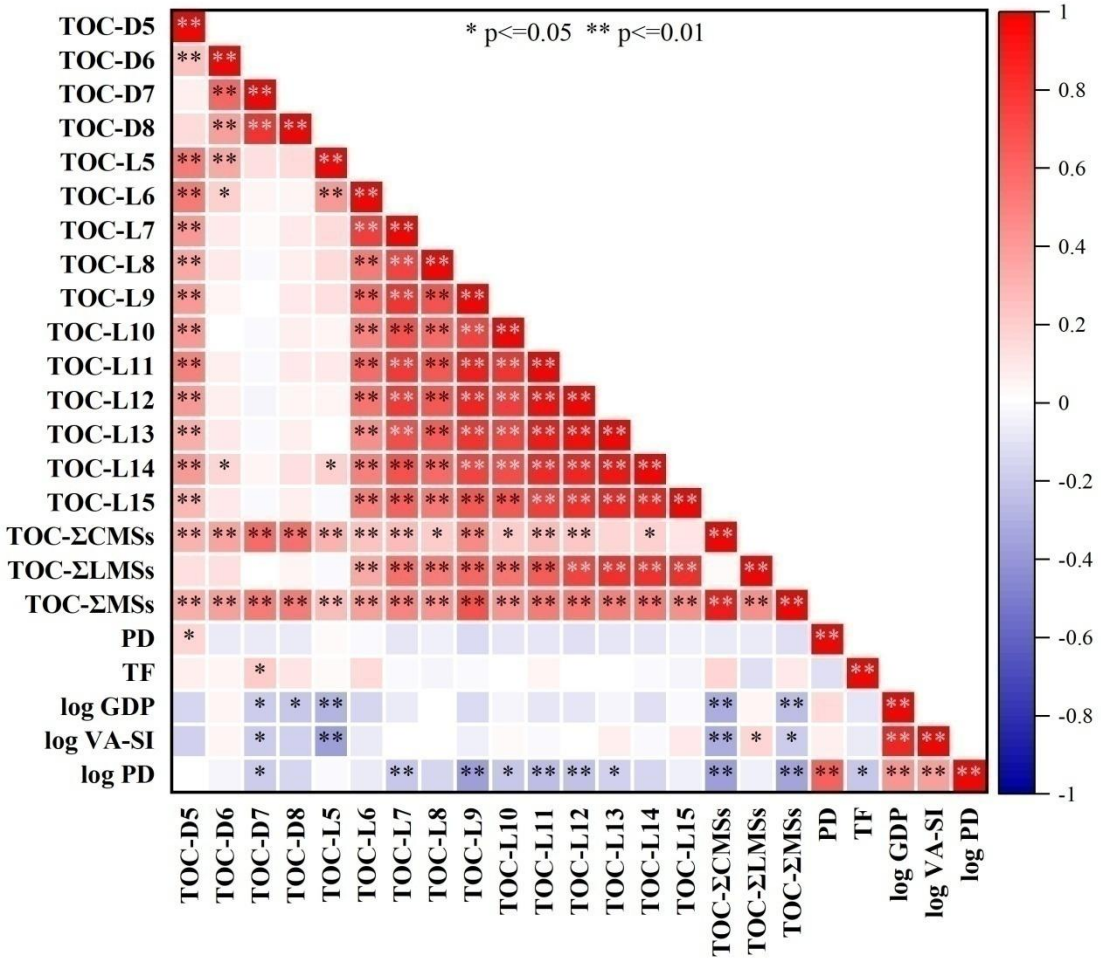

Fig. S10 Correlation analysis among the concentrations of methylsiloxanes normalized to the total organic carbon (TOC) in road dust samples, gross domestic product (GDP), value added of the secondary industry (VA-SI), traffic flow (TF), and the population density (PD) in sampled cities in China.

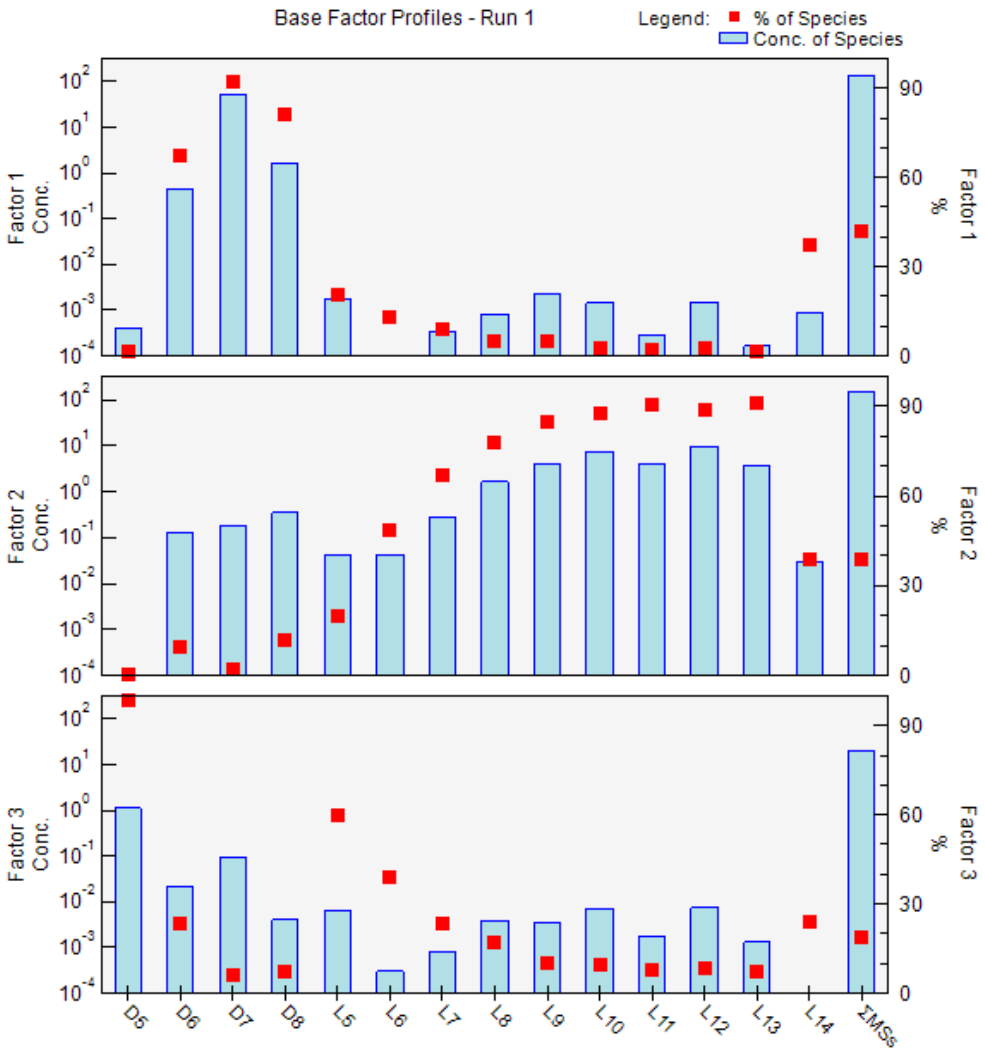

Fig. S11 Concentrations and profiles of methylsiloxanes species in each factor and contribution to each source.

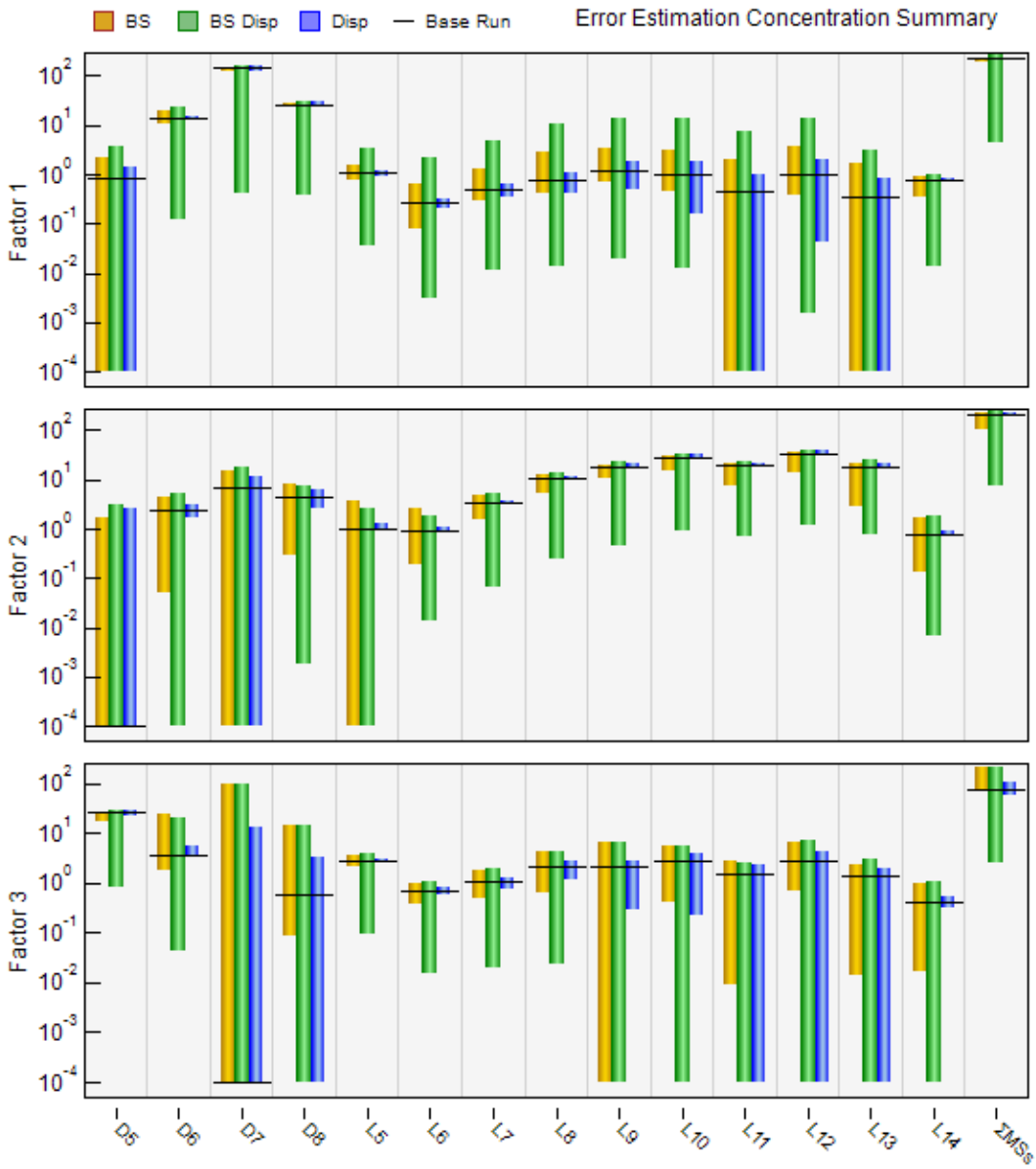

Fig. S12 Error estimation concentration summary plot.

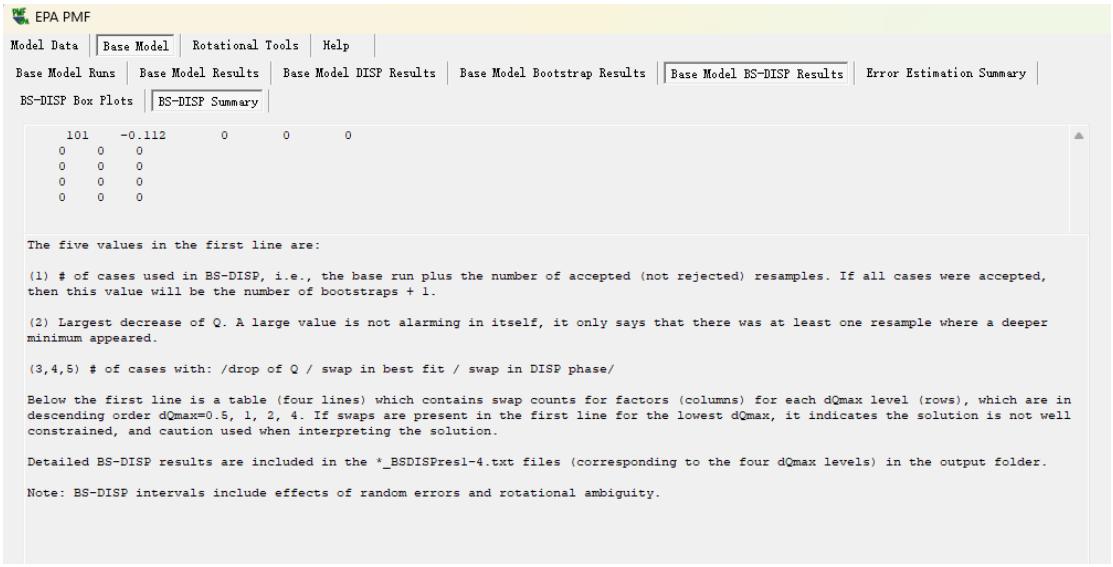

Fig. S13 The Base Model BS-DISP Summary screen.

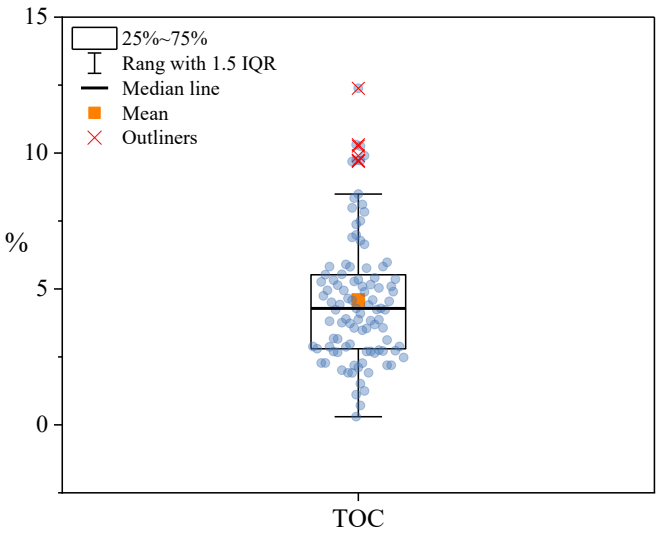

Fig. S14 Box plot of TOC values in road dust.

References

Capela D, Alves A, Homem V, Santos L (2016). From the shop to the drain — Volatile methylsiloxanes in cosmetics and personal care products. Environment International, 92-93: 50–62

Chen W, Oh J-S, Lim J-E, Moon H-B (2023). Occurrence, time trends, and human exposure of siloxanes and synthetic musk compounds in indoor dust from Korean homes. Ecotoxicology and Environmental Safety, 266: 115538

Cheng J, Tang Z, Ma Y, Yin H, Meng T, Sun J (2021a). Methyl siloxanes in road dust from a large silicone manufacturing site in China: implications of human exposure. Environmental Science and Pollution Research, 28(13): 16054–16064

Cheng J, Tang Z, Ma Y, Yin H, Meng T, Sun J (2021b). Methyl siloxanes in soils from a large silicone-manufacturing site, China: concentrations, distributions and potential human exposure. Environmental Geochemistry and Health, 43(10): 3871–3881

Dudzina T, Von Goetz N, Bogdal C, Biesterbos J W H, Hungerbühler K (2014). Concentrations of cyclic volatile methylsiloxanes in European cosmetics and personal care products: Prerequisite for human and environmental exposure assessment. Environment International, 62: 86–94

Feng J, Liu M, Zhao J, Hu P, Zhang F, Sun J-H (2019). Historical trends and spatial distributions of polycyclic aromatic hydrocarbons in the upper reach of the Huai River, China: Evidence from the sedimentary record. Applied Geochemistry, 103: 59–67

Feng J, Zhang F, Zhao J, Guo W, Sun J (2018). An improved quantification method for 12 linear dimethylsiloxanes and 1 cyclic dimethylsiloxane in polydimethylsiloxane using gas chromatography-flame ionization detector : Development strategy and accuracy. Journal of Chromatography A, 1578: 112–116

Fromme H, Witte M, Fembacher L, Gruber L, Hagl T, Smolic S, Fiedler D, Sysoltseva M, Schober W (2019). Siloxane in baking moulds, emission to indoor air and migration to food during baking with an electric oven. Environment International, 126: 145–152

Horii Y, Kannan K (2008). Survey of organosilicone compounds, including cyclic and linear siloxanes, in personal-care and household products. Archives of Environmental Contamination and Toxicology, 55(4): 701–710

Horii Y, Nojiri K, Minomo K, Motegi M, Kannan K (2019). Volatile methylsiloxanes in sewage treatment plants in Saitama, Japan: Mass distribution and emissions. Chemosphere, 233: 677–686

Li L, Chang R, Li J, Zhang H, Du X, Li J, Yuan G-L (2024). Assessing the impact of mining on cyclic and linear methylsiloxane distribution in Tibetan soils: Source contribution and transport pattern. Science of The Total Environment: 173542

Liu N, Sun H, Xu L, Cai Y (2021). Methylsiloxanes in petroleum refinery facility: Their sources, emissions, environmental distributions and occupational exposure. Environment International, 152: 106471

Lu Y, Yuan T, Wang W, Kannan K (2011). Concentrations and assessment of exposure to siloxanes and synthetic musks in personal care products from China. Environmental Pollution, 159(12): 3522–3528

Lu Y, Yuan T, Yun S H, Wang W, Wu Q, Kannan K (2010). Occurrence of Cyclic and

Linear Siloxanes in Indoor Dust from China, and Implications for Human Exposures. Environmental Science & Technology, 44(16): 6081–6087
Meng T, Su S, Cheng J, Zhong F, Tang Z (2021). Methylsiloxanes in street dust from Hefei, China: Distribution, sources, and human exposure. Environmental Research, 201: 111513
Niu H, Su X, Li Q, Zhao J, Hou M, Dong S, Yan X, Sun J, Feng J (2023). Dimethylsiloxanes in dust from nine indoor microenvironments of Henan Province: Occurrence and human exposure assessment.Science of The Total Environment, 903: 166546
Sánchez-Brunete C, Miguel E, Albero B, Tadeo J L (2010). Determination of cyclic and linear siloxanes in soil samples by ultrasonic-assisted extraction and gas chromatography–mass spectrometry. Journal of Chromatography A, 1217(45): 7024–7030
Sofowote U M, Mccarry B E, Marvin C H (2008). Source Apportionment of PAH in Hamilton Harbour Suspended Sediments: Comparison of Two Factor Analysis Methods. Environmental Science & Technology, 42(16): 6007–6014
Tran T M, Abualnaja K O, Asimakopoulos A G, Covaci A, Gevao B, Johnson-Restrepo B, Kumosani T A, Malarvannan G, Minh T B, Moon H B, Nakata H, Sinha R K, Kannan K (2015). A survey of cyclic and linear siloxanes in indoor dust and their implications for human exposures in twelve countries. Environment International, 78: 39–44
Tran T M, Kannan K (2015). Occurrence of cyclic and linear siloxanes in indoor air from Albany, New York, USA, and its implications for inhalation exposure. Science of The Total Environment, 511: 138–144
Tran T M, Tu M B, Vu N D (2018). Cyclic siloxanes in indoor environments from hair salons in Hanoi, Vietnam: Emission sources, spatial distribution, and implications for human exposure. Chemosphere, 212: 330–336
Us Epa O (2015). EPA Positive Matrix Factorization 5.0 Fundamentals and User Guide
Wang J, Li G, Zhang Z, Huang Q, Niu B, Zhang Y, Long D (2024). Detailed insights of polydimethylsiloxane (PDMS) degradation mechanism via ReaxFF MD and experiments. Chemical Engineering Journal, 488
Wang R, Moody R P, Koniecki D, Zhu J (2009). Low molecular weight cyclic volatile methylsiloxanes in cosmetic products sold in Canada: Implication for dermal exposure. Environment International, 35(6): 900–904
Wei T, Wijesiri B, Li Y, Goonetilleke A (2020). Particulate matter exchange between atmosphere and roads surfaces in urban areas. Journal of Environmental Sciences (China), 98: 118–123
Zhu Y, Tang Z, He Y, Wang F, Lyu Y (2023). Occurrence of methylsiloxanes in indoor store dust in China and potential human exposure. Environmental Research, 218: 114969